www.lajss.org
Latin American Journal of Solids and Structures 1 (2003) 3-24

Structural topology optimization considering material failure constraints and multiple load conditions

Eduardo Alberto Fancello[a,*], Jucélio Tomás Pereira[b]

[a]Departamento de Engenharia Mecânica,
Universidade Federal de Santa Catarina,
Florianópolis, SC, Brasil
[b]Departamento de Engenharia Mecânica,
Centro Federal de Educação Tecnológica do Paraná,
Curitiba, PR, Brasil

Abstract

This work presents an approach for mass minimization of mechanical devices subject to multiple load conditions and material failure constraints. The design control is performed through topology optimization concepts, in particular the SIMP approach (Solid Isotropic Microstructure with intermediate mass Penalization). The optimization procedure combines an Augmented Lagrangian technique to handle local stress-based failure constraints and a box-type algorithm to deal with upper and lower limits on the design variables. Sensitivity analysis calculations are performed through analytical expressions using the adjoint technique. In this way, numerical costs associated with a multiple loaded case are very similar to those of a single loaded case. Some numerical examples are presented showing quite different optimal designs if we compare single and multiple load cases.

Keywords: Structural optimization, topology optimization, multiple load conditions, material failure constraints

1 Introduction

The design of mechanical devices that use the least material possible but are capable of performing their function without material failure is a common goal in industrial applications. Topological optimization is perhaps today's most flexible numerical tool available to perform a systematic search for this kind of design. The literature associated with this research area shows several approaches to solving this problem and, despite not being rigorous, two groups of techniques may be distinguished.

The first one contains those formulations in which a classical optimization problem is set and its solution obtained through mathematical programming techniques (we include in this group

* Corresponding author Email: fancello@grante.ufsc.br Received 4 Aug 2003; In revised form 2 Nov 2003

genetic based algorithms and their combinations with directional algorithms). The second group includes those approaches that define a local criterion to update the design variables. This last group may be subdivided in two subgroups: those related to optimality conditions based upon sensitivity information and those based on heuristic constructions. Moreover, the criterion is called local if the design change at a particular material point depends on information only from the neighborhood of that point.

Formulations from the first group hold a clear mathematical structure and their solution guarantees the satisfaction of the optimization statement. They are also quite flexible in the sense that they allow different types of constraints and cost functions. They have the computational cost of solving a mathematical programming problem in which the evaluation of cost function, constraints and their derivatives (if necessary) involves the solution of equilibrium equations. In addition, convergence problems may arise.

Algorithms from the second group (in particular heuristic based and fully-stressed based) may present simplicity of implementation and relatively low computational costs. However, their main drawback is that the final design will not necessarily satisfy the original optimization requirements.

Only a few studies dealing with mass minimization and material failure constraints in continuum structures may be found in literature within the first approach. Among them we can mention Duysinx & Bendsøe [7], Duysinx & Sigmund [8], Stolpe & Svanberg [18], Pereira [12] and Pereira et al. [13].

At first, this problem appears a little naive; however, a couple of particular characteristics make it quite troublesome. Firstly, the consideration of local stress constraints implies (in the discretized formulation) the use of a number of them, proportional to the number of elements, which should be large enough to obtain an appropriate characterization of the stress field. Secondly, and most importantly, stress based failure constraints are associated with the singularity-stress phenomenon, whose efficient treatment is still the subject of research (Sved & Ginos [21], Kirsch [11], Cheng & Guo[6], Rozvany [17] and Stolpe & Svanberg [19][20]).

This study is based on the first approach, with particular focus on the the consideration of multiple loads.

Devices subject to multiple load cases is the most common situation in mechanics. In general, the optimal design of a device sumitted to a single load case show a poor, or not admissible behavior if a different load pattern is applied. Multiple load conditions are usually treated by multiobjective optimization within the compliance problem; the objective function is a weighted combination of the compliances of each load condition. However, the choice of the appropriate weighting parameters is quite arbitrary. In evolutionary or fully-stressed type algorithms, multiple loads are frequently treated by including some heuristics in the local criterion in order to take into account the mechanical response due to each load. On the other hand, the mathematical problem of mass minimization subject to local material failure constraints and multiple load cases is just a natural extension of that with a single load case. No additional heuristic or weighting function definition is needed. Moreover, it will be seen that numerical costs associated

with a multiple loaded problem are not necessarily much greater than those of a single loaded case.

For a given domain Ω, the problem to be solved is

$$\begin{array}{ll} \text{Minimize} & \text{Mass} \\ \text{Subject to :} & F_i\left(\sigma_i\left(\mathbf{x}\right)\right) \leq 0, \quad \forall \ \mathbf{x} \in \Omega, \quad i = 1...N, \end{array} \tag{1}$$

where F_i is a material failure function related to the stress field $\sigma_i\left(\mathbf{x}\right)$ in equilibrium with the corresponding i-th load case. N is the number of load cases. It is well known that (1) is ill-posed and its direct treatment is therefore not appropriate. Thus, several techniques are used to circumvent this problem. This study formulates (1) in the same way as developed in Duysinx & Bendsøe [7], i.e. combining the SIMP technique and a local material failure constraint. The numerical approach, however, is quite different and follow the principles used in Pereira et al. [13]. In order to keep this paper self contained and allow the inclusion of the multiple load condition within the expressions, the next three sections are dedicated to presenting briefly the formulation and its numerical approach. Section 5 presents numerical examples in which optimal designs for multiple loaded structures are analyzed.

2 Formulation

For the sake of simplicity, state equations are restricted to linear elasticity where a body Ω is submitted to contact forces $\bar{\mathbf{t}}$ and known displacements $\bar{\mathbf{u}}$ on its boundary, as shown in Figure 1.

As in most topological problems, we distinguish the material part Ω_m of Ω and the void region Ω_v. Let $\mathbf{u}$, $\varepsilon(\mathbf{u})$ and $\sigma(\mathbf{u})$ be the displacement, strain and stress fields and $\mathbf{D}$ the elasticity tensor. We then have the following boundary value problem:

$$\begin{aligned} \sigma(\mathbf{u}) = \mathbf{D}\varepsilon(\mathbf{u}) &= \mathbf{D}\nabla^{\mathbf{S}}\mathbf{u} \ , \\ \text{div } \sigma(\mathbf{u}) &= \mathbf{0} \qquad \forall\, \mathbf{x} \in \Omega \ , \\ \sigma\ \mathbf{n} &= \bar{\mathbf{t}} \qquad \forall\, \mathbf{x} \in \partial\Omega_N \subset (\partial\Omega_m \cap \partial\Omega) \ , \\ \sigma\ \mathbf{n} &= \mathbf{0} \qquad \forall\, \mathbf{x} \in \partial\Omega_F := \partial\Omega_m \backslash (\partial\Omega_N \cup \partial\Omega_D) \ , \\ \mathbf{u} &= \bar{\mathbf{u}} \qquad \forall\, \mathbf{x} \in \partial\Omega_D \subset (\partial\Omega_m \cap \partial\Omega) \ . \end{aligned} \tag{2}$$

Using the SIMP artificial microstructure (Solid Isotropic Microstructure with Penalty for intermediate materials, Bendsøe & Sigmund [2], the design space includes a continuous variation of material between solid ($\rho = 1$) and void ($\rho = 0$). The constitutive behavior depends on the relative density ρ and the solid material elasticity tensor $\mathbf{D}$ through the following expression:

$$\mathbf{D}_\rho = f_D\left(\rho\right)\mathbf{D} = \rho^p\mathbf{D}, \tag{3}$$

$$\sigma = \mathbf{D}_\rho\varepsilon \ . \tag{4}$$

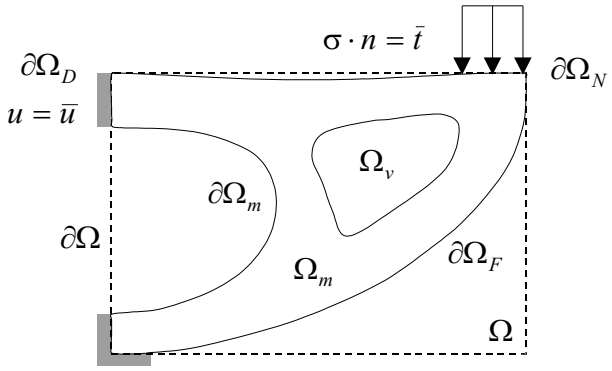

Figure 1: Geometric definitions of a domain composed by solids and voids.

The effective stress tensor $\bar{\sigma}$ for an arbitrary intermediate material is set to be greater than the homogenized stress σ and dependent on the original (solid material) elasticity tensor and on the apparent (homogenized) value of deformation [7]:

$$\bar{\sigma} = \mathbf{D}\,\varepsilon\,. \tag{5}$$

For a given effective stress tensor $\bar{\sigma}$, an equivalent scalar stress σ_e (for example, von Mises) is computed. With this value, a failure function is defined as

$$F\left(\bar{\sigma}\right) = \frac{\sigma_e}{\sigma_{adm}} - 1 \leq 0, \tag{6}$$

where σ_{adm} is the material yielding stress or maximum admissible value.

When density goes to zero, high deformations may occur due to low stiffness and consequently, high but finite local effective stress values are computed. This phenomenon, known as Stress Singularity, is characterized by introducing a discontinuity in the failure function for null values of ρ. The ϵ-regularization technique proposed by Cheng & Guo [6] is used to overcome this inconvenience through the following re-definition of the failure function:

$$\begin{cases} g\left(\mathbf{x}\right) \equiv \rho\left(\mathbf{x}\right) F\left(\bar{\sigma}\left(\mathbf{x}\right)\right) - \epsilon\left(1 - \rho\left(\mathbf{x}\right)\right) \leq 0, & a.e.\ in\ \Omega\ , \\ 0 < \epsilon^2 = \rho_{\min} \leq \rho\left(\mathbf{x}\right) \leq 1, & \forall\ \mathbf{x} \in \Omega. \end{cases} \tag{7}$$

The optimization problem is then posed as the minimization of the functional $m\left(\rho\right)$ subject to a set of local failure constraints:

$$\underset{\rho \in W_{\rho}^{1,2}(\Omega)}{\text{Min}}\ m\left(\rho\right) = \int_{\Omega} \rho\, d\Omega + \frac{1}{2} r_{\rho} \int_{\Omega} f_{\rho}\left(\rho\right)\ d\Omega + r_m \int_{\Omega} f_m\left(\rho\right)\ d\Omega \tag{8}$$

$$\text{Subject to}: g_i\left(\mathbf{x}\right) = g(\rho\left(\mathbf{x}\right), \bar{\sigma}_i\left(\mathbf{x}\right)) \leq 0 \quad a.e.\ in\ \Omega, \quad i = 1...N,$$

where

$$f_\rho(\rho) = (\nabla\rho)^T(\nabla\rho)\ ,$$
$$f_m(\rho) = \rho(1-\rho)\ ,$$
$$W_\rho^{1,2}(\Omega) = \left\{\rho \mid \rho \in W^{1,2}(\Omega);\ 0 < \rho_{\min} \le \rho(\mathbf{x}) \le 1\ \forall\ \mathbf{x} \in \Omega\right\}$$

Among several alternatives to avoid the checkerboard phenomenon (limit on the perimeter, Petersson [14], limit on the difference of density between adjacent elements, Bendsøe [1], Petersson & Sigmund [15]) we took advantage of a continuum approach for the density control and included the second term of $m(\rho)$, which is a penalization of the density gradients (Pereira et.al, [12], Borrval[5]). This choice is in accordance with the proposed approach and it showed to be a simple and effective stabilizer of the checkerboard phenomenon.

The third term introduces an explicit penalization of the intermediate densities. Constants r_m and r_ρ are the corresponding penalization factors.

Aiming to obtain numerical solutions, an Augmented Lagrangian functional is defined, adding to the cost function a penalization on the stress constraints. Defining $g_i(\rho, \bar{\sigma})$, we have

$$\pounds(\rho;\lambda,\mathbf{r}) = m(\rho) + \sum_{i=1}^{N} m_i(\rho;\lambda_i,r_i) = m(\rho) + \sum_{i=1}^{N}\int_\Omega M(\rho;\lambda_i,r_i)\,d\Omega, \tag{9}$$

$$M(\rho;\lambda_i,r_i)\,d\Omega = \frac{1}{r_i}\max\left\{g_i\left[\lambda_i r_i + \frac{1}{2}g_i\right];\ -\frac{(r_i\lambda_i)^2}{2}\right\}. \tag{10}$$

The penalization functional $m_i(\rho;\lambda_i,r_i)$ for the i-th load case consists of linear and quadratic terms of the failure function g_i that are multiplied by a penalization parameter $r_i > 0$ and by a Lagrangian function $\lambda_i \in L^2(\Omega)$. The derivation of M_i follow the classic Augmented Lagrangian procedure for a general inequality constraint (see Bertsekas [3]).

Thus, for a given set $\mathbf{r}^k = \{r_1^k, r_2^k, ..., r_N^k\} > 0$ and $\lambda^k = \{\lambda_1^k, \lambda_2^k, ..., \lambda_N^k\}$, $\lambda_i^k, \in L^2(\Omega)$, the following box-constrained problem can be solved for each k-th iteration:

$$\underset{\rho\in W_\rho^{1,2}(\Omega)}{\text{Min}}\ \pounds\left(\rho;\lambda^k,\mathbf{r}^k\right) \tag{11}$$

The solution of the whole optimization problem is obtained by solving a sequence of subproblems (11) with an appropriate updating of parameters $\lambda^k, \mathbf{r}^k$. In this approach the standard Augmented Lagrangian updating rule was chosen [3]:

$$\lambda_i^{k+1} = \max\left\{\lambda_i^k + \frac{1}{2}g_i\,;\,0\right\},\ \ r_i^{k+1} = \frac{r_i^{k+1}}{t},\ \ t > 1\ . \tag{12}$$

3 Sensitivity Analysis

The algorithm chosen to solve problem (11) needs information of first order derivatives of the Lagrangian functional. Detailed operations to obtain analytical expressions of these gradients are found in [13]. The directional (Gateaux) derivative of the objective functional $\pounds\left(\rho;\lambda^k,\mathbf{r}^k\right)$ for fixed and known values of λ^k and $\mathbf{r}^k$ is given by:

$$\dot{\pounds}\left(\rho;\lambda^k,\mathbf{r}^k\right)[y]=\dot{m}\left(\rho\right)[y]+\sum_{i=1}^{N}\dot{m}_i\left(\rho;\lambda_i^k,r_i^k\right)[y], \tag{13}$$

where

$$\dot{m}\left(\rho\right)[y]=\int_\Omega\left[1+r_m\frac{df_m\left(\rho\right)}{d\rho}+\frac{1}{2}r_\rho\frac{df_\rho\left(\rho\right)}{d\rho}\right]y\,d\Omega, \tag{14}$$

$$\dot{m}_i\left(\rho;\lambda_i^k,r_i^k\right)[y]=m_i'\left(\rho;\lambda_i^k,r_i^k\right)[y]-B'(\mathbf{u}_i,\mathbf{u}_i^a)[y]+l'(\mathbf{u}_i^a)[y]\ , \tag{15}$$

$$\begin{aligned}m_i'\left(\rho;\lambda_i^k,r_i^k\right)[y]&=\int_\Omega\frac{\partial M_\sigma\left(\rho;\lambda_i^k,r_i^k\right)}{\partial\rho}\,y\,d\Omega\,,\\&=\int_\Omega\left\{\frac{1}{r_i^k}\left[F\left(\sigma_i\right)+\epsilon\right]\left\langle g_i+r_i^k\lambda_i^k\right\rangle^+\right\}\,y\,d\Omega\,.\end{aligned} \tag{16}$$

In these expressions, y is a variation of ρ, $\mathbf{u}_i$ is the displacement field for the i-th load case and $\mathbf{u}_i^a$ is the adjoint solution for the i-th adjoint problem associated with the corresponding load case. The operator $\langle\cdot\rangle^+$ returns the positive part of the argument. The first term, $m(\rho)$, depends explicitly on density ρ and obtaining its derivative is straightforward. The penalization terms $m_i\left(\rho;\lambda_i^k,r_i^k\right)$ are implicitly dependent on ρ through the mechanical solutions $\mathbf{u}_i\left(\rho\right)$ for each load case. Their derivatives are obtained by the adjoint method [10]). The partial (Gateaux) derivative of B for fixed real displacements $\mathbf{u}_i$ and adjoint solution $\mathbf{u}_i^a$ is given by

$$\begin{aligned}B'\left(\mathbf{u}_i,\mathbf{u}_i^a\right)[y]&=\lim_{t\to0}\left[\frac{B_{\rho+ty}\left(\mathbf{u}_i,\mathbf{u}_i^a\right)-B_\rho\left(\mathbf{u}_i,\mathbf{u}_i^a\right)}{t}\right]\\&=\int_\Omega q\rho^{(q-1)}\left[\mathbf{D}\nabla^S\mathbf{u}_i\cdot\nabla^S\mathbf{u}_i^a\right]\,y\,d\Omega\,.\end{aligned} \tag{17}$$

Furthermore, it is assumed (for the sake of simplicity) that external loads do not depend on ρ and then $l_i'\left(\mathbf{u}_i^a\right)[y]=0$. The solution $\mathbf{u}_i^a$ is computed from the classical expression of the adjoint problem:

$$B\left(\mathbf{u}_i^a,\mathbf{v}\right)=\int_\Omega\left(\frac{\partial M_i}{\partial\nabla^S\mathbf{u}}\cdot\nabla^S\mathbf{v}\right)d\Omega\,,\quad\forall\ \mathbf{v}\in V, \tag{18}$$

$$=\int_\Omega\left(\frac{\rho}{r_i^k}\left\langle g_i\left(\mathbf{x}\right)+r_i^k\lambda_i^k\right\rangle^+H^{\sigma i}\cdot\nabla^S\mathbf{v}\right)d\Omega\,,\quad\forall\ \mathbf{v}\in V, \tag{19}$$

where $H^{\sigma i}$ is a second order tensor obtained explicitly from the material failure criterion evaluated for the current stress state $\sigma_i = \sigma(\mathbf{u}_i)$.

As it is widely known, computing the gradient of the cost function using adjoint approach, has almost the same computational cost of a single analysis. It must be noted, however, that if each local stress constraint is considered separately (in order to use it in a general algorithm for constrained minimization), its individual gradient will also be required, increasing computational costs. This is not the case for the present approach, where stress constraints are included in the cost function, and their local character is achieved with appropriate actualization of the Lagrange multipliers during iterations.

4 Discretization and numerical procedure

The present implementation is limited to 2D problems although the formulation holds for 3D problems as well. Due to its flexibility in mesh generation and low computational costs, the classical three-node Lagrangian element was used to solve the boundary value problem. The same shape functions are used to define a continuous density field ρ whose nodal values play the role of design variables. The checkerboard phenomenon, common in low-order elements, is easily stabilized with the density gradient penalization term. The failure function is evaluated at each element centroid. Thus, the number of design variables is proportional to the number of nodes while the number of stress constraints is proportional to the number of elements (which in triangular meshes is approximately twice the number of nodes)

As proposed in Section 2, the Augmented Lagrangian procedure is used, which requires the solution of a sequence of minimization subproblems. For the k-th subproblem, a set of Lagrangian multipliers and penalization factors $(\lambda^k, \mathbf{r}^k)$ is set and the minimization of the objective functional $\mathcal{L}(\rho; \lambda^k, \mathbf{r}^k)$ subject to side constraints is performed. This sequence is as follows:

1. Define $k = 0$, r_m, r_ρ, λ^k and $\mathbf{r}^k$;
2. Minimize the functional $\mathcal{L}\left(\rho; \lambda^k, \mathbf{r}^k\right)$, $0 < \rho_{\min} \leq \rho\left(\mathbf{x}\right) \leq 1$;
3. Verify convergency within a tolerance. If satisfied, stop the process;
4. Update η^k, λ^k, $\mathbf{r}^k$;
5. $k = k + 1$, Return to Step 2.

The optimization algorithm used in Step 2 is a non-linear trust-region algorithm proposed by Friedlander et al., [9]. This algorithm was generalized by Bielschowsky et al. [4] and it is based on the construction of a quadratic subproblem defined on a trust region.

An adaptive strategy is also used based on the quality of the approximated subproblem that modifies the size of the trust region to accelerate convergence. The results of this work were obtained with an implementation of this algorithm, called BOX-QUACAN, provided by its authors and parametrically adapted to the present case.

5 Numerical Results

This section is devoted to showing some results comparing optimal designs due to different load cases and their combination. As almost every optimization problem, some parameters must be set. The penalization of checkerboard parameter r_ρ, has a strong influence on the topological complexity. The bigger the parameter the simplest the topology with a rough boundary definition is obtained. Parameter r_m is used to penalize intermediate densities, but it was noted that the influence of it is quite smaller than that of r_ρ. Another important parameter is ϵ; in general, more robust designs are obtained for smaller values of ϵ and vice versa, which is in accordance with the nature of this parameter. Theoretical considerations and numerical examples analyzing the the influence of $r_m, r_\rho, \lambda^k, \mathbf{r}^k$ and ϵ on numerical results are found in [13]. In the present examples the following values were used, unless specified: $r_m = 0.95$, $r_\rho = 0.001$, $\mathbf{D}_\rho = \rho^3\mathbf{D}$, $\epsilon^2 = \rho_{\min} = 0.01$.

5.1 Traction and bending of a beam

This simple example exploits many particularities of the present formulation and highlights some polemic aspects such as the fully stressed design condition. An analogous example was shown in [13] but no multiple loaded case was analyzed. The background domain is a square beam with symmetry boundary conditions on the left side and traction and bending forces on the right side (see Figure 2). The value for the traction forces is $t_t = 17.5\,Pa$ and that for the bending forces is $t_b = 30\ Pa$. The stress limit is $\sigma_{adm} = 35Pa$. Other parameters are $E = 100\,Pa$ and $\nu = 0.3$. Two regions are distinct; the left one is submitted to optimization while the right one is fixed. Figure 3 shows the final design for the first load case in which a bar with half the transversal section of the original bar is obtained. A fully stressed design condition is fulfilled on the left side of the bar while a smooth, not fully-stressed transition is found on the right side. A different design is obtained for the "pure-bending" case (Figure 4). Material is spread up and down in order to increase the moment of inertia of the cross section. The failure function is saturated only at the extreme lower and upper boundaries. This is a didactic case where a fully-stressed design condition cannot be achieved: further elimination of material, even in a non saturated region, will produce inadmissible stress values at upper/lower boundaries of the beam. The consideration of both loads (not simultaneously applied) is shown in Figure (5). It is possible to see that the cross section is again half the size of the original one in order to support traction forces. Two bars remain at the "flanges" of the beam, but a different transition with the fixed part of the beam was obtained. In addition, as traction can bend the "flanges", a thin vertical column is inserted to avoid this movement. Figures 6 and 7 show the ϵ-relaxed failure function of this final design for each of the two load cases.

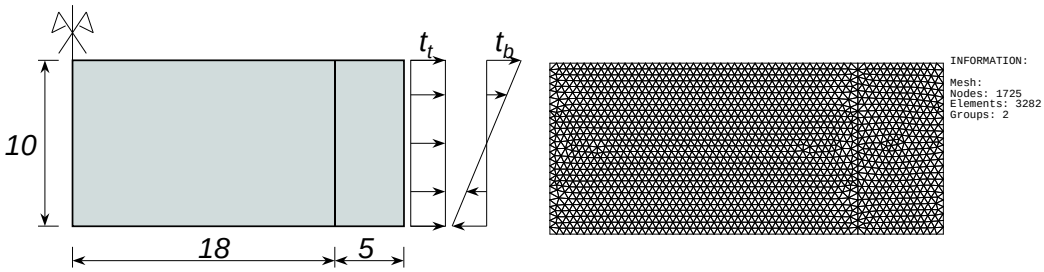

Figure 2: Traction and bending of beam.

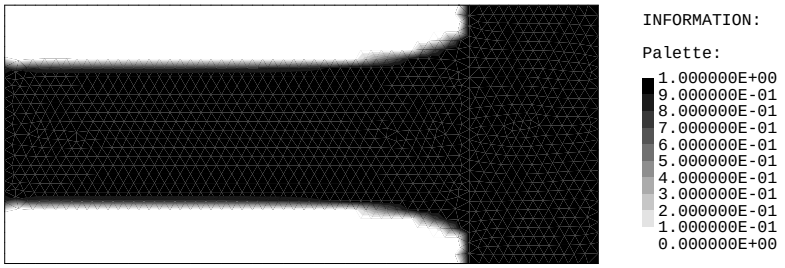

Figure 3: Density distribution for traction load.

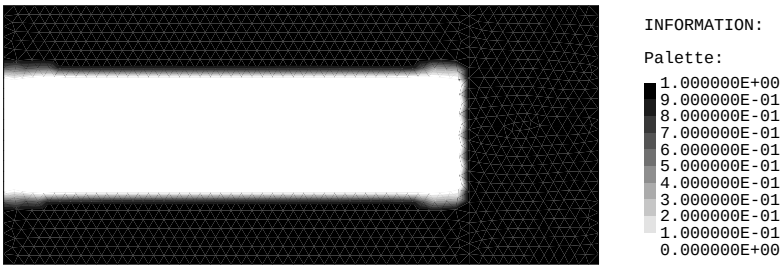

Figure 4: Density distribution for bending load.

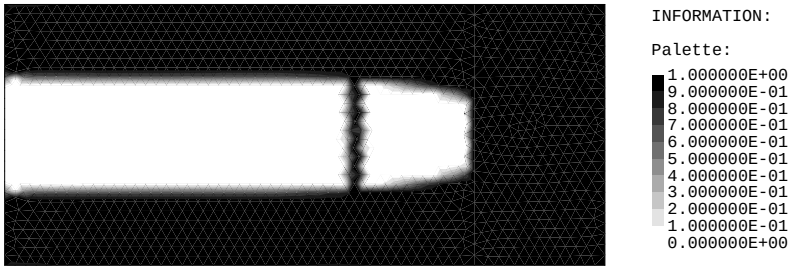

Figure 5: Density distribution for traction and bending loads.

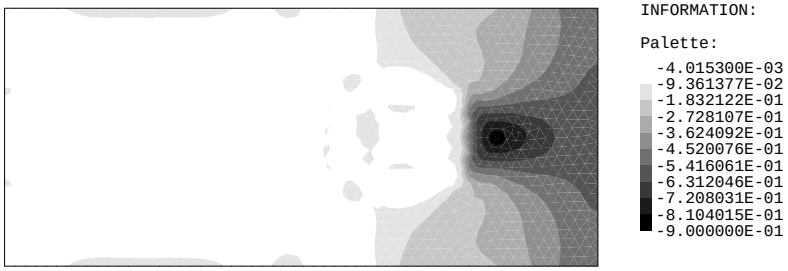

Figure 6: Multiple load case design. ϵ-relaxed failure function for traction load.

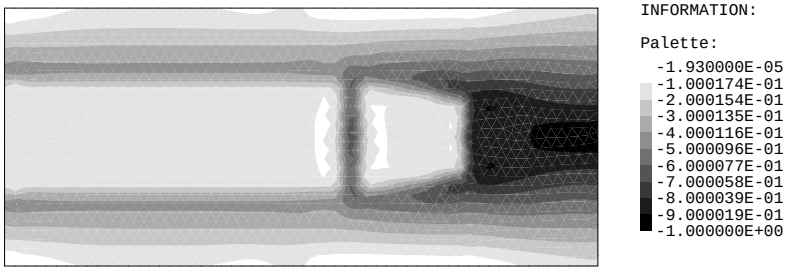

Figure 7: Multiple load case design. ϵ-relaxed failure function for flexion load.

5.2 Anisotropic failure criterion

This example shows a case in which the failure function behaves differently in traction than in compression. The failure function is defined by Raghava's model (Raghava et al.[16]) and the example consists of a squared background mesh submitted to a distributed force applied on a small region at the bottom with fixed density (see Figure 8). The upper boundary is clamped. The same load is applied in up, down, left and right directions. The value of the total force is $P_1 = P_2 = P_3 = P_4 = 1N$. The admissible stress in traction is $\sigma^t_{adm} = 2.5\,Pa$ and in compression $\sigma^c_{adm} = 7.5\,Pa$. Material parameters are $E = 100\,Pa$, $\nu = 0.3$ and $L = 1m$. Figure 9 show the final design for Load 1. As expected, the bar under traction has a wider cross section. Similar behavior occurs for the third and fourth loads in the vertical direction. Figures 10 and 11 show the final design for Load 3 (compression) and Load 4 (traction). The final density distribution due to the four loads individually applied is presented in Figure 12. It is possible to see that this topology and shape is quite similar to that of the first load but with both bars having the same thickness, which is clearly a consequence of failure constraints to loads 1 and 2. The ϵ-relaxed failure function of this final design for loads 1 and 3 are shown in Figures 13 and 14.

5.3 Constrained domain

This example can be classified as belonging to those cases in which the background domain introduces an initial geometric constraint. This type of problem is perhaps the most common

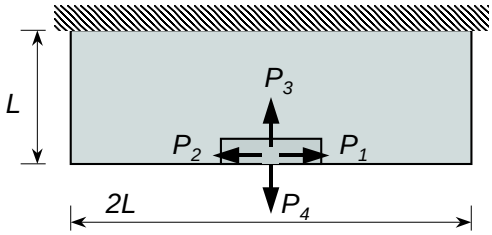

Figure 8: Anisotropic failure function.

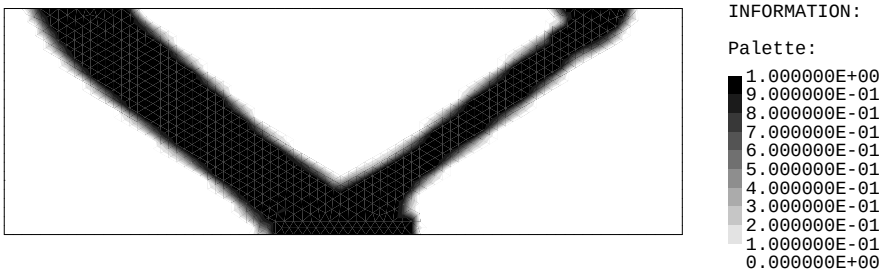

Figure 9: Density distribution for load 1.

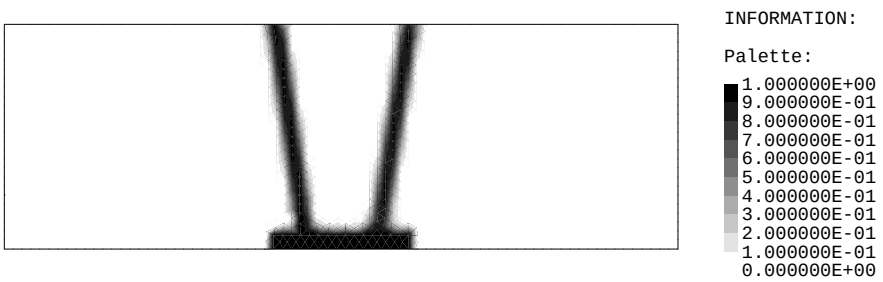

Figure 10: Density distribution for load 3.

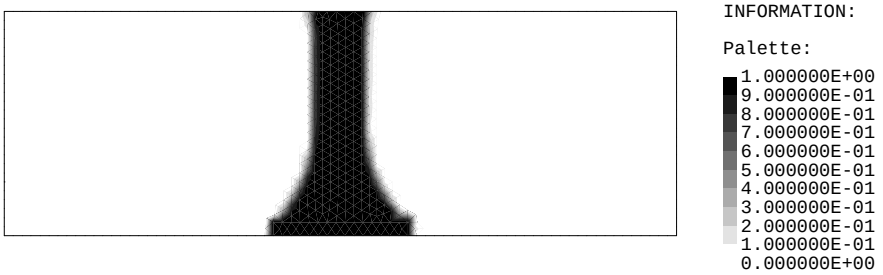

Figure 11: Density distribution for load 4.

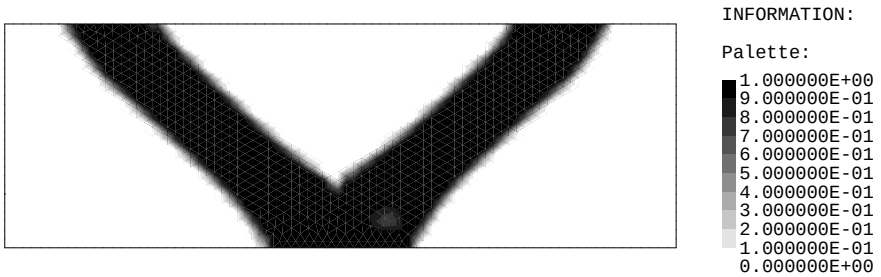

Figure 12: Density distribution for multiple load conditions (loads 1 to 4).

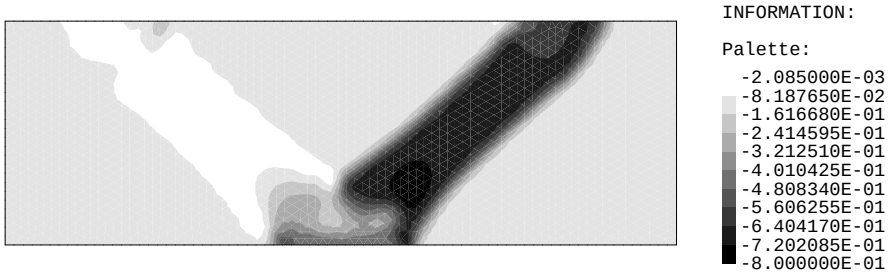

Figure 13: Multiple load case. ϵ-relaxed failure function for load 1.

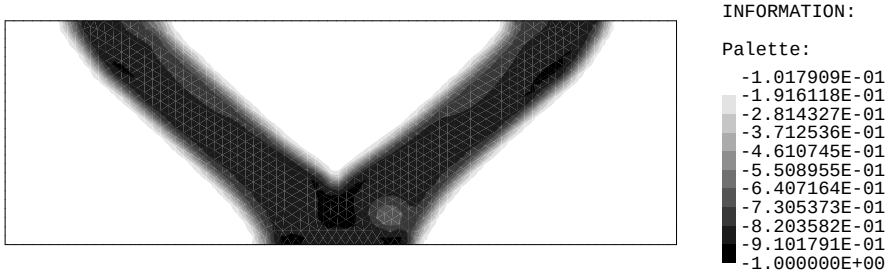

Figure 14: Multiple load case. ϵ-relaxed failure function for load 4.

case in practical applications: the final design must fit into the space available.

Due to the existence of a singular stress point at the inner corner of the L-shaped initial background domain, the present case may be used as a benchmark for those formulations that seek the satisfaction of failure constraints; the algorithm should find a final shape avoiding these initial stress concentrations. Two loads are applied on a small fixed region at the right side of the initial domain (see Figure 15). The solution for the vertical load was considered in [13] and it is shown in Figure 16a. Material and geometric data are $E = 100Pa$, $\nu = 0.3$, $L = 1.0\,m$, $\sigma_{adm} = 42.42\,Pa$ and $P_1 = P_2 = 1.0\,N$. The final designs for load 2 and for the multiple load case are shown in figures 16b and 17. Comparing the solution for the vertical load case with that for the multiple load case it is possible to see the accentuation of the radius close to the inner initial corner as well as the the growth of the cross section near the clamped boundary due to bending stresses produced by the horizontal load.

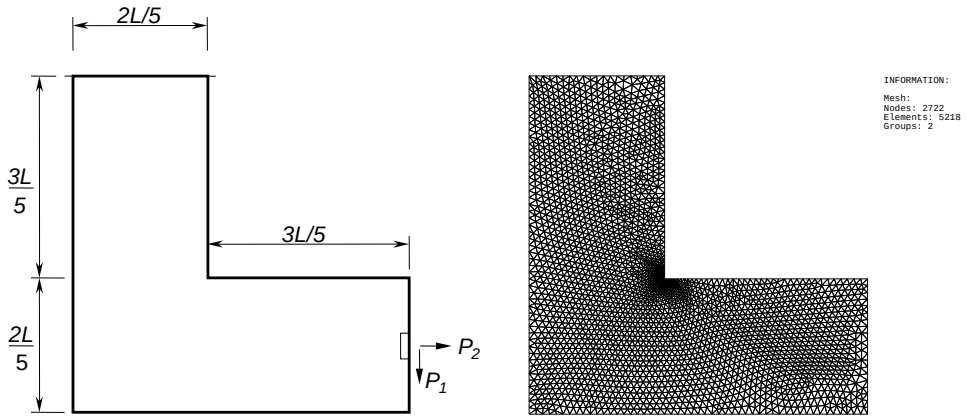

Figure 15: Constrained domain.

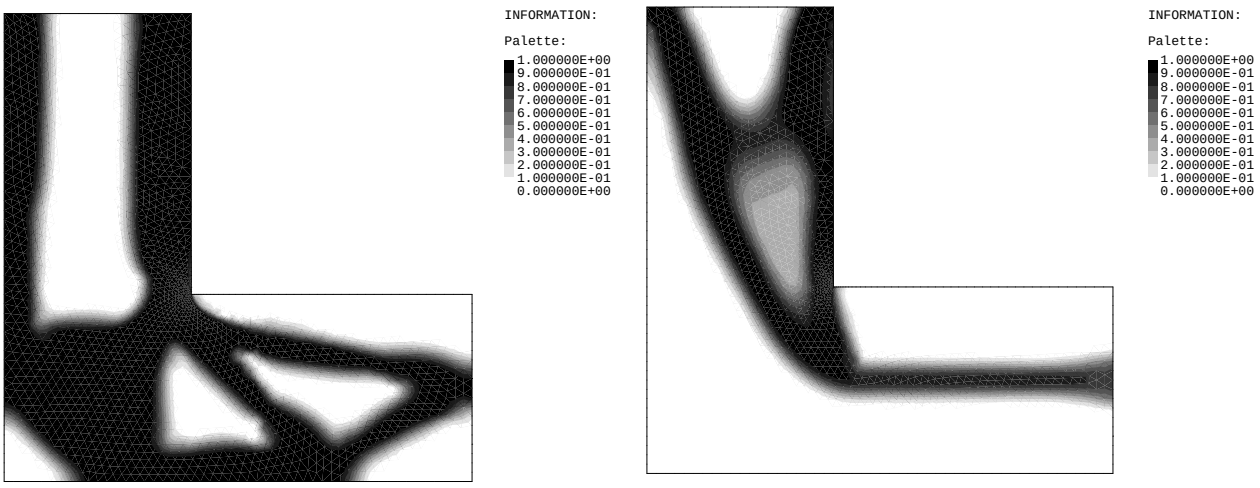

Figure 16: Density distribution for a) load 1 and b) load 2

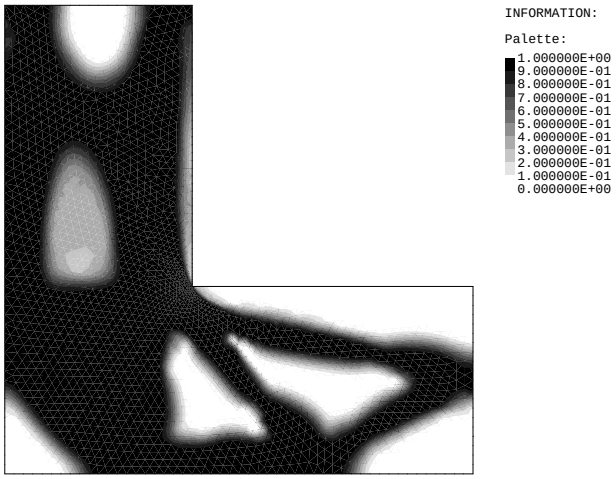

Figure 17: Density distribution for multiple load case.

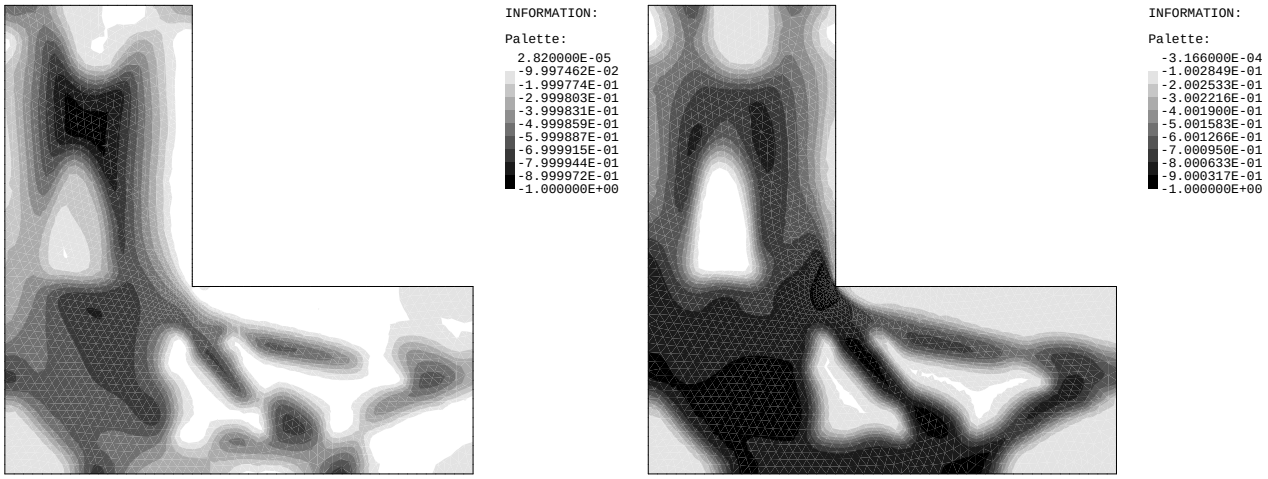

Figure 18: Multiple load case. ϵ-relaxed failure function for a) load 1, b) load 2.

5.4 Device with a dovetail joint

Previous examples are academical, but appropriate to illustrate the characteristics of the present formulation. The present example shows a more realistic application, performed to guide the design of a plastic device manufactured by Tigre Tubos e Conexões S.A., Brazil (FINEP, Verde-Amarelo Project). It also illustrates the importance of allowing multiple load cases in practical simulations.

The problem consists of a component fixed with a dovetail joint and submitted to a load applied in four different directions on a hole created to fit a shaft (Figure 19). Each load produces different contact conditions on the dovetail, which enforces quite different optimal designs for each case. To handle this problem in a precise way, the formulation should be extended to incorporate state equations involving contact conditions. Nevertheless, a shortcut is taken here. The problem is substituted by a simpler one considering the hole fixed and four different loads on the dovetail (Figure 19). Three regions not submitted to optimization were defined. The first one is a ring around the hole. The remainder define the dovetail shape and the support the applied loads. Material properties used in this run (different form those used in the plastic device) are $E = 200000\,MPa$, $\nu = 0.3$, $\sigma_{adm} = 150\,MPa$ and the thickness of the device is $40\,mm$. The loads of the simplified case are distributed along their surface and their values are (Figure 19) $f1 = 3150\,N$, $f2.1 = 11860\,N$, $f2.2 = 11040\,N$ and $f3 = 4500\,N$.

Figures 21 and 22 show the final design for loads 1, 2, 3 and for the multiple load case (solution for load 4 is symmetrically equivalent to the solution for load 2). It is interesting to note that design 1 is completely different to design 3, which is contrary to that initially expected. Loads in the third case "open" the dovetail due to traction. A design with vertical bars like that of the first load case would fail due to the bars bending. Instead, a strong curved beam is

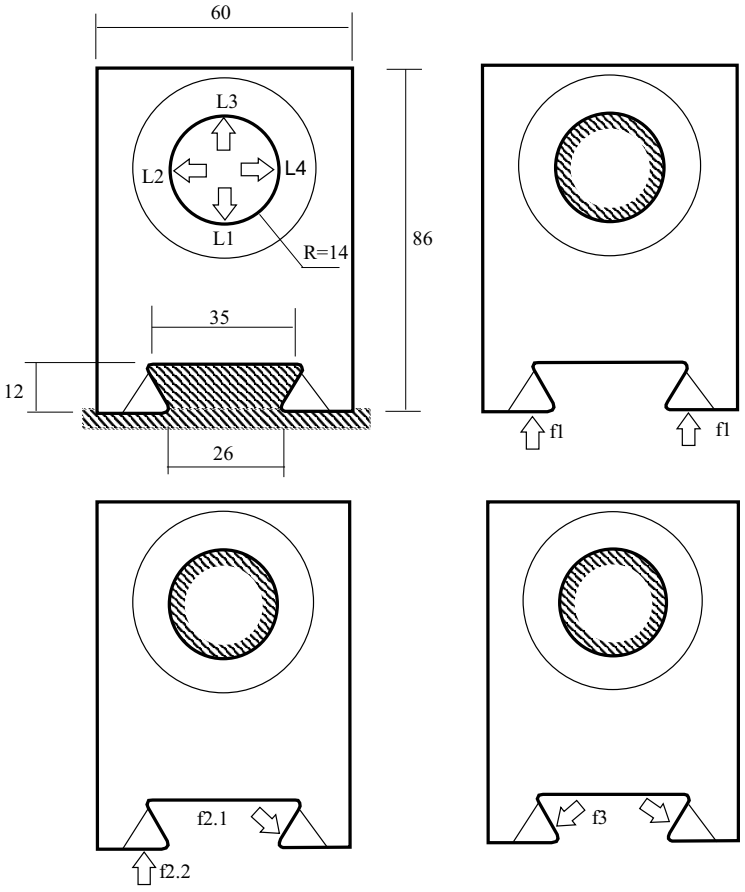

Figure 19: Model.

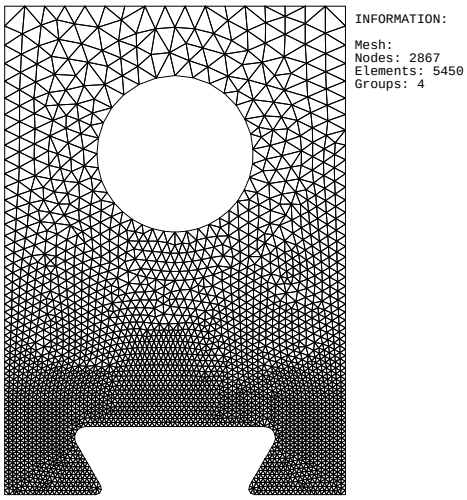

Figure 20: Mesh.

formed and its length reaches the optimal value for the new thin vertical bars.

Figures 23a and 23b show the ϵ-relaxed failure function for load case 3 and for the multiple load case under load 4, respectively. The final design for the multiple load case is a frame-like structure with transversal sections dimensioned in order to satisfy local failure constraints. Once again, we must remark that this is not the solution for the original problem, but seems to be an adequate initial design for it.

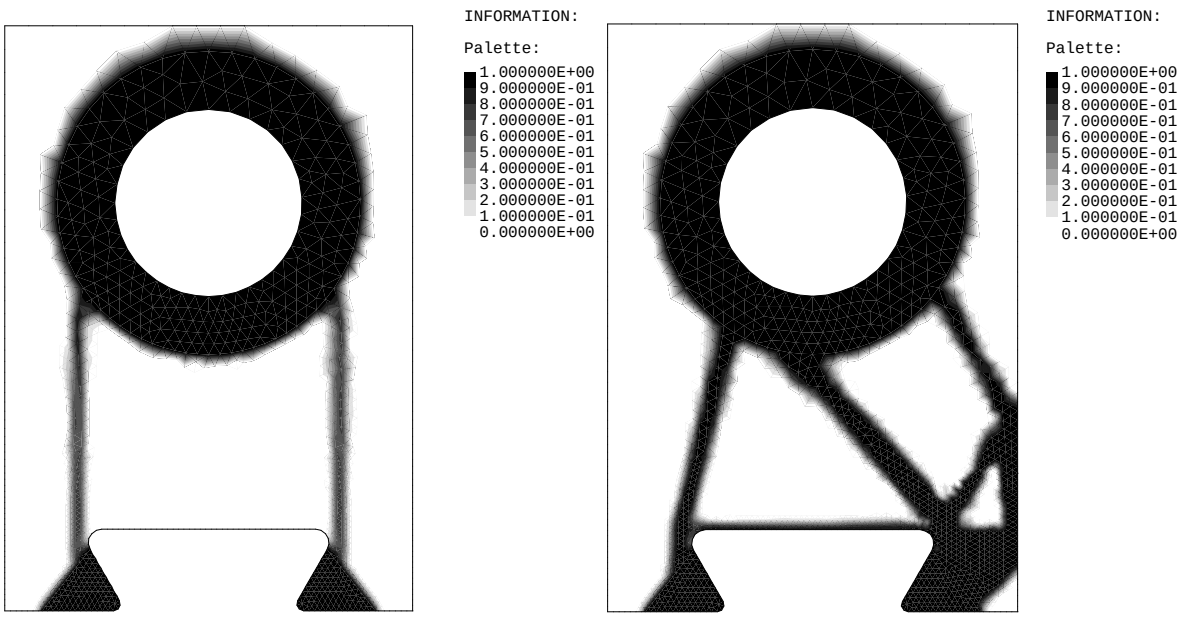

Figure 21: Density distribution for a) load 1 and b) load 2.

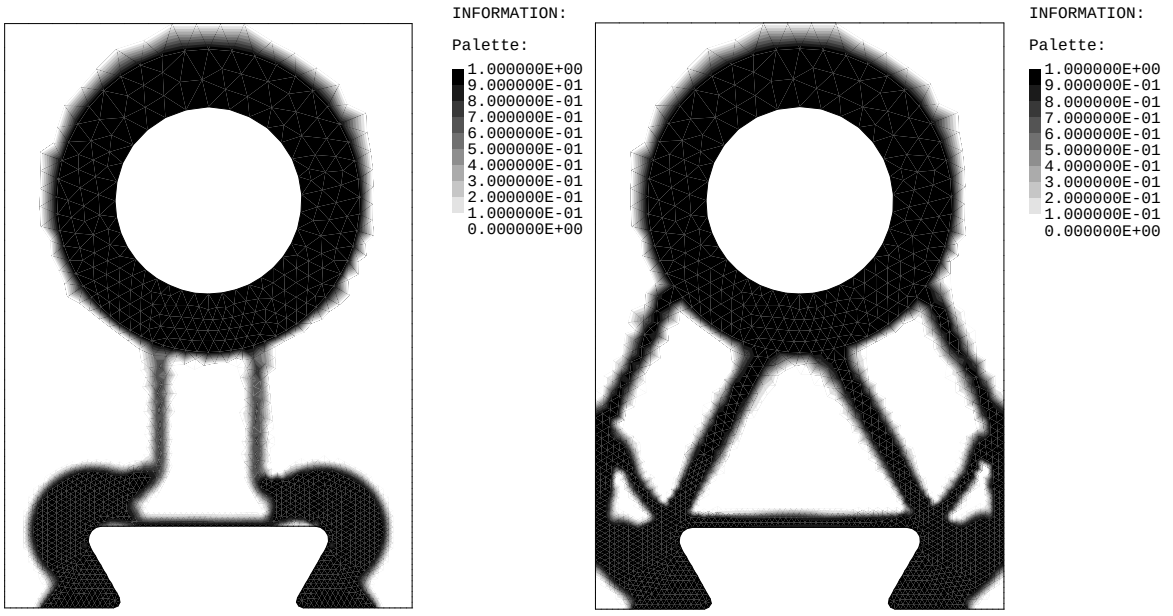

Figure 22: Density distribution for a) load 3 and b) multiple (not simultaneous) loads.

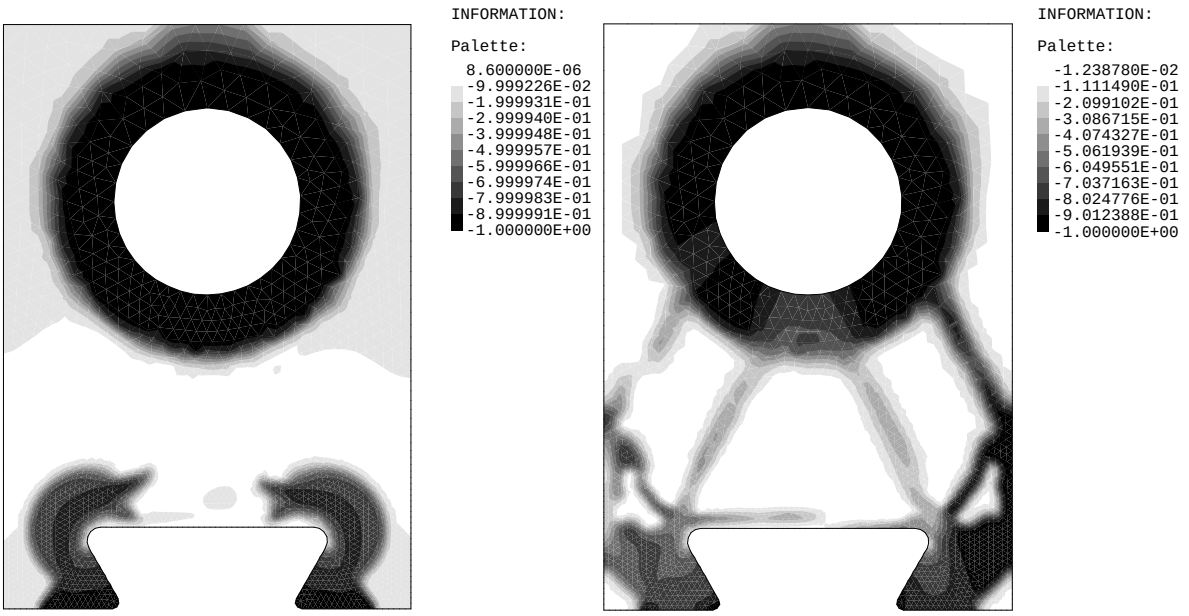

Figure 23: ϵ-relaxed failure function for a) design for load 3, b) design for multiple loads under load 4.

6 Final remarks

This paper discusses the consideration of multiple load cases in a formulation oriented to minimize the mass of a mechanical component subject to material failure constraints. The theoretical principles of the problem are briefly outlined. Some final considerations should be highlighted:

- The numerical results show, as expected, significative differences in design for each load. Also, the final design that satisfies failure constraints for all individual loads shows a topology that is not just an "envelope"of each individual design (as is most commonly expected).
- From a numerical point of view it is claimed that, for the present formulation, the computational effort spent on considering failure constraints due to multiple loads is not much greater than that for of single load case; if the same essential boundary conditions are considered, the same triangularized stiffness matrix is used for each load case and, consequently, solutions and adjoint solutions for gradient computations are easily performed for each load case by back-substitution operations. Numerical performance confirms these conclusions.

- The approach was shown to be quite robust. If we consider that problem 4 has 5450 elements and 4(four) independent load cases, this means a total of 21800 stress constraints. Figures of ϵ-relaxed failure functions show that these constraints are fulfilled throughout the domain.

- Local optimum designs are, in most cases, not fully stressed. The first example clearly shows that the existence of this condition depends on the mechanical problem. Multiple load conditions therefore lead to designs which are far from being fully stressed due to one load in particular.

- In spite of the of quite good results obtained, convergence problems still appear. One must first note that it is quite simple to formulate a problem with no solution; for a given load there is no guarantee of the existence of an admissible domain within the space available. Also, due to the large number of stress constraints, the problem has plenty of local optimal solutions. The Augmented Lagrangian approach in combination with the ϵ-relaxed procedure can be seen as a possible strategy to drive the solution to points near the global optima. The work of Stolpe & Svanberg [20] presents clear considerations about local and global solutions in the use of epsilon-regularizations.

- Real problems submitted to different loads usually produce different contact regions and load transmissions in mechanical devices. This problem is clearly shown by the fourth example in which a substitute simplified problem was analyzed to circumvent the contact problem. However, this issue deserves more attention and appropriate formulations for its treatment.

Acknowledgments: The authors are grateful to Ana Friedlander, Sandra A. Santos and José M. Martínez (IMECC/UNICAMP) for the BOX-QUACAN algorithm and its implementation. We thank also to the group TACSOM (Theoretical, Applied and Computational Solid Mechanics Group) (www.lncc.br) for the computational facilities provided by ACDPOOP/ACDPFEM system. This work was partially supported by CNPq, project number 551549/2002-5, and FINEP - Verde Amarelo project.

References

[1] M.P. Bendsøe. Optimization of Structural Topology, Shape, and Material. Springer Verlag, Berlin, Alemanha; Heidelberg, Alemanha; New York, EUA; etc., 1995.

[2] M.P. Bendsøe and O. Sigmund. Material interpolation schemes in topology optimization. Archive of Applied Mechanics, 69:635–654, 1999.

[3] D.P. Bertsekas. Constrained Optimization and Lagrange Multiplier Methods. Athena Scientific, Belmont, MA, EUA, 1996.

[4] R.H. Bielschowsky, A. Friedlander, F.A.M. Gomes, J.M. Martínez, and M. Raydan. An adaptive algorithm for bound constrained quadratic minimization. Investigación Operativa, 7:67–102, 1997.

[5] T. Borrvall. Topology optimization of elastic continua using restriction. Archives on Computational Methods in Engineering, 190:4911–4928, 2001.

[6] G.D. Cheng and X. Guo. ε–Relaxed approach in structural topology optimization. Structural Optimization, 13:258–266, 1997.

[7] P. Duysinx and M.P. Bendsøe. Topology optimization of continuum structures with local stress constraints. International Journal for Numerical Methods in Engineering, 43:1453–1478, 1998.

[8] P. Duysinx and O. Sigmund. New developments in handling stress constraints in optimal material distribution. In 7th AIAA/USAF/NASA/ISSMO Symposium on Multidisciplinary Design Optimization, pages 98/4906/1–9, Saint Louis, MI, EUA, 1998. American Institute of Aeronautics and Astronautics.

[9] A. Friedlander, J.M. Martínez, and S.A. Santos. A new trust-region algorithm for bound constrained minimization. Applied Mathematics and Optimization, 30(3):235–266, 1994.

[10] E.J. Haug, K.K. Choi, and P.V. Komkov. Design Sensitivity Analysis of Structural Systems. Academic Press, Orlando, FL, EUA, 1986.

[11] U. Kirsch. On singular topologies in optimal structural design. Structural Optimization, 2:133–142, 1990.

[12] J. T. Pereira. Otimização Topológica de Componentes Mecânicos com Restrições sobre o Critério de Falha Material. Ph.d. thesis, GRANTE – Grupo de Análise e Projeto Mecânico – Departamento de Engenharia Mecânica – Universidade Federal de Santa Catarina, Florianópolis, SC, Brasil, 2001.

[13] J. T. Pereira, E.A. Fancello, and C. S. Barcellos. Topology optimization of continuum structures with material failure constraints. Structural and Multidisciplinary Optimization, (to be published), 2003.

[14] J. Petersson. Some convergence results in perimeter-controlled topology optimization. Computer Methods in Applied Mechanics and Engineering, 171:123–140, 1999.

[15] J. Petersson and O. Sigmund. Slope constrained topology optimization. International Journal for Numerical Methods in Engineering, 41:1417–1434, 1998.

[16] R. Raghava, R.M. Caddell, and G.S.Y. Yeh. The macroscopic yield behaviour of polymers. Journal of Materials Science, 8:225–232, 1973.

[17] G.I.N. Rozvany. On design dependent constraints and singular topologies. Structural and Multidisciplinary Optimization, 21:164–172, 2001.

[18] M. Stolpe and K. Svanberg. Modelling topology optimization problems as mixed 0-1 programs. Internal Report KTH/OPT SYST/FR 01/10 SE, KTH – Optimization and Systems Theory – Department of Mathematics – Royal Institute of Technology, Stockholm, Suécia, October 2001.

[19] M. Stolpe and K. Svanberg. On the trajectories of penalization methods for topology optimization. Structural and Multidisciplinary Optimization, 21(2):128–139, 2001.

[20] M. Stolpe and K. Svanberg. On the trajectories of the epsilon–relaxation approach for stress–constrained truss topology optimization. Structural and Multidisciplinary Optimization, 21(2):140–151, 2001.

[21] G. Sved and Z. Ginos. Structural optimization under multiple loading. International Journal of Mechanical Science, 10:803–805, 1968.